Indirect electrode or direct electrode?: A revisitation of electrode configuration in simulated lightning damage testing

Yakun Liu [a,b,*], Cien Xiao [a], Siyuan Shen [a], Yeqing Wang [c], Earle Williams [b]

[a] *Key Laboratory of Control of Power Transmission and Conversion, Ministry of Education, Department of Electrical Engineering, Shanghai Jiao Tong University, Shanghai, 200030, China*
[b] *Department of Civil and Environmental Engineering, Massachusetts Institute of Technology, Cambridge, Massachusetts, 02139, USA*
[c] *Department of Mechanical and Aerospace Engineering, Syracuse University, Syracuse, NY, 13244, USA*

ARTICLE INFO

ABSTRACT

The damaged area and depth of materials caused by lightning are key parameters in laboratory lightning testing, but these results are influenced by the experimental setup. This work studies the advantages and drawbacks of the use of a direct electrode or indirect electrode by combining experimental results and numerical modeling. Using the indirect electrode, the impacts of the arc energy and over-pressure wave are constrained by the dielectric electrode head. Net emission coefficient, electrical and thermal conductivity of arc channel are altered with added metal vapor from the ignition wire. These reasons lead to milder damaged area and depth of materials in lightning testing. Using the direct electrode overcomes the aforementioned deficiencies but faces an obstacle of self-melting. A special tungsten-copper electrode may be taken as a compromised solution. This work contributes to diminishing the misinterpretation from the testbed in laboratory lightning certification.

1. Introduction

Lightning is a kind of intense natural discharge that inflicts serious or even catastrophic damage to oil tanks, aircraft, electric power transmission lines, *etc.*[1–4]. For instance, aircraft is struck by lightning on average once every 3,000 h of its flight time [5]. Therefore, lightning-vulnerable targets are subjected to a series of laboratory tests to evaluate their lightning tolerance, in which the lightning damage testing of materials is one of the principal examinations [6–8]. Damage effects of lightning on materials (*e.g.* melting, eroding, deforming, burning, etc.) originate from complicated multi-physical interactions of the overloaded current/voltage, massive heating, intense electromagnetic forces, and overpressures [7,9–11]. To quantify the damage level, the damaged area and depth of materials are commonly examined. Recently, these parameters are found to be affected by the experimental configuration [9,12,13], bringing questionable assessment and misinterpretation to the design of lightning protection.

Considering the uncertainty of lightning strikes, the simulated lightning technology in laboratory is the only feasible method for lightning damage evaluation on materials. Whereas, for typical natural lightning, the available electrical voltage reaches as high as $\sim 10^8$ V and is accompanied by currents with amplitude to ~ 200 kA [1,2]. Such

extraordinarily high power exceeds the power ratings of capacitors and it is still impracticable to reproduce both the high voltage and large current simultaneously. Therefore, the existing lightning simulation method mainly satisfies the current parameters but compromises the output voltage in the material testing, which limits the arc discharge length to several centimeters and brings the testbed dependence of the material lightning damage testing to the experimental configuration.

To address the influence imposed by the experimental setup, this work first focuses on the electrode configuration used in simulated lightning damage testing. The benefits and drawbacks of the use of a direct electrode or an indirect electrode are studied by a combination of simulated lightning experiments and numerical modeling. For the indirect electrode configuration, we analyze the influence from the electrode head and ignition wire on the damaged area and depth of materials to lightning. For the direct electrode configuration, the anti-erosion ability of electrode materials is analyzed to serve as guidance in the selection of electrode material. Comparisons of natural and simulated lightning are detailed in Section 2. Analyses on the indirect and direct electrodes are presented in Section 3. Conclusions are stated in Section 4.

---

* Corresponding author.
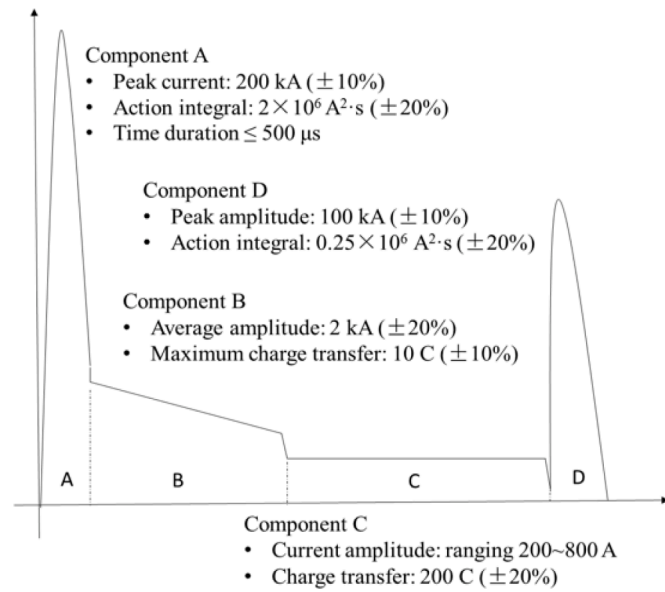*E-mail address:* lysky00@sjtu.edu.cn (Y. Liu).

Fig. 1. The set of A/B/C/D waveforms in the simulated lightning currents [19].

2. Comparison of natural and simulated lightning

Lightning develop from ordinary thunderstorm clouds based on the main mechanism of the non-inductive charge separation involving ice particle collisions [14,15]. In a typical negative flash, the discharges initiate with the preliminary breakdown (PB) within cloud and evolve into the stepped leader (SL). The average leader current is usually 100~1000 A with current peaks larger than 1 kA. The depletion of negative charge during the PB and SL processes induce a huge electric potential gradient and promote the leader development, triggering the return stroke with a peak current as large as 200 kA (even higher). Between successive strokes, K- and J- processes occur in cases of the additional charge available within cloud. The dart leader with a peak current of ~1 kA and charge of ~1 C propagates downward along or off-track the residual discharge channel to initiate subsequent strokes. These subsequent strokes exhibit a peak current up to ~100 kA with a fast zero-to-peak risetime, which is usually intermittent with continuing currents with a magnitude of tens to hundreds of amperes and a duration lasting up to hundreds of milliseconds. Meanwhile, the continuing currents occasionally have several superimposed M-components [8].

A rough estimate of the electrical energy available in the lightning generation is the product of the initial charge storage transported from cloud-to-ground and an electrostatic potential difference ($Q \cdot V/2$), which is of the order of 5×10^9 J in total (~10^2 C $\times 10^8$ V/2) and a corresponding energy per unit channel length of 10^6 J/m [16]. The peak effective power is about 10^{11} W/m with the associated electric field intensity of ~10^6 V/m in the return stroke, assuming the current rise-time is tens of microseconds. The intense energy released by the return strokes heats the discharge channel to increase its temperature rapidly to ~30,000 K and creates high pressure at an order of 10 atmospheres or more. The discharge channel will expand at a supersonic speed and generate an outward propagating wave in a roughly cylindrical shape as the instantaneous overpressure exceeds the magnetic pressure from the plasma pinch. Meanwhile, the acoustic radiation (also known as 'shock wave') is emitted at a peak acoustic pressure of several N/m² with hundreds of milliJoule per cubic meter of acoustic energy (mJ/m³) at a distance of 70 m with a peak current of tens of kiloamperes measured in an artificially-triggered lightning stroke [17]. This channel expansion takes about 5~10 μs and finally forms a high-temperature and low-density plasma in a physical state of quasi-thermodynamic equilibrium.

Current parameters of lightning are measured and quantified with

Table 1
Parameter analyses of the typical impulse currents with the double exponential model.

Waveform	1/20μs	4/10μs	8/20μs	18/40μs	30/80μs
Charge transfer/C	5.6	2.3	3.9	10.1	16.5
Action integral/ A²·s	0.6×10^6	0.3×10^6	0.5×10^6	1.4×10^6	2.2×10^6

their salient electromagnetic signatures. A set of A/B/C/D waveforms, as shown in Fig. 1, are recommended in lightning testing in the SAE standard to represent the multiple lightning currents [18,19]. Component A, representing the initial return stroke, is reproduced with a peak amplitude of 200 kA and an action integral of 2×10^6 A²·s with a risetime less than 50 μs and a total duration of less than 500 μs. Component B, representing the intermediate current, is simulated by a unidirectional square-waveform current with an average amplitude of 2.0 kA and a duration of less than 5 ms. Component C, representing the long continuing current, makes use of the unidirectional rectangular-waveform current with a duration of 250~1000 ms and an adjustable amplitude of 200~800 A. Component D, representing the subsequent strokes, is mimicked by an impulse current with an action integral of 0.25×10^6 A²·s at a current amplitude of 100 kA and a risetime shorter than 25 μs. These current parameters are selected in the consideration of the 5% exceedance values in lightning currents with both the positive and negative polarity.

In the lightning simulation, a variety of waveforms, such as 4/10 μs, 1.2/50 μs, 1/20 μs, 18/40 μs, 30/80 μs, and 8/20 μs waveforms, have been employed to represent Component A in the damage testing of lightning. Whereas, not all the waveforms are in good agreement with the parameters of an impulse current with a peak amplitude of 200 kA (±10%) and action integral of 2×10^6 A²·s (±20%) with a risetime less than 50 μs and a total duration less than 500 μs. Based on the double exponential model in Eq. (1) (commonly used in the description of the channel base lightning current) [20], a quantitative comparison of the parameters with a current amplitude of 200 kA in the above waveforms is shown in Table 1.

$$i(t) = (I_{\max} / \eta)\left(e^{-t/\tau_1} - e^{-t/\tau_2}\right) \tag{1}$$

where $I_{\max}$ is the peak current amplitude, η is the correction factor. τ_1 and τ_2 are the time constants involved in the current rise-time and decay-time, and also influence the current steepness.

Results show that, the 30/80 μs waveform satisfies the parameter requirement of the first return stroke (Component A) both in the rise-time/duration and action integral at a current amplitude of 200 kA. The 4/10 μs waveform can represent the subsequent stroke (Component D) in fulfillment of an action integral of 0.25×10^6 A²·s (±20%) at a current amplitude of 100 kA (±10%) with a risetime shorter than 25 μs. The intermediate current (Component B) can be simulated by a unidirectional square-waveform current with an average amplitude of 2.0 kA (±20%) and a duration of less than 5 ms (±10%). For the reproduction of the long continuing current (Component C), it is recommended to use the unidirectional rectangular-waveform current with a duration of 250~1000 ms and an adjustable amplitude of 200~800 A.

Cloud-to-ground lightning has multiple strokes during a flash (12 strokes in the 5% exceedance value). The interstroke interval is 115 ms on average between 50%~5% exceedance for multiple strokes. However, the present standards cut off the time interval between strokes (see Fig. 1) and confine currents in a specific sequence (A/B/C/D in turn). In natural lightning, the continuing currents generally occur after the subsequent return strokes, which fall short of the stroke sequences mentioned in the standards. It is also noted that the existed lightning testings usually adopt a single impulse current, due to the output limitation of the lightning simulation generator used. The single current testing allows samples cooling down, unrepresentative to the continuous
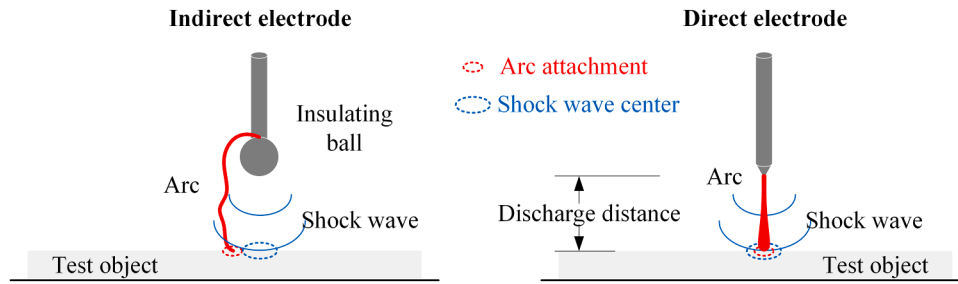
Fig. 2. Indirect electrode (left) and direct electrode (right).

damage in natural lightning. Fortunately, with the development of the lightning simulation generator, it is feasible to produce multiple impulse currents in the laboratory now [9]. Therefore, the adoption of multiple strokes with a representative sequence and time intervals is recommended for the lightning damage testing.

To generate the impulse currents with such a large amplitude of 200 kA, the output voltage of generators is usually restricted to tens of kilovolts due to a limitation of the power rating of the capacitor, much smaller than the electrical potential difference ($\sim 10^8$ V) in lightning. The typical output voltage of the capacitor is ~ 30 kV and the resultant peak electric field strength is $\sim 10^6$ V/m, a factor of 10^3 times lower than the counterpart of lightning. The simulated lightning arc generated by self-breakdown has been proven to show a satisfactory consistency with the natural lightning arc with regard to the spectral lines in the ultraviolet-visible-infrared region (invariant with the arc length) [21], in which the atomic spectrum of nitrogen, hydrogen, and oxygen are expected to be prominent. This suggests that the laboratory and natural lightning arcs are very similar to each other in the underlying discharge mechanisms. The arc resistance is on the order of tens of ohm per meter. Thus, a peak power ($I^2 \cdot R$) of $\sim 10^{11}$ W/m is foreseen for the return stroke in a simulated lightning arc, consistent with the peak effective power of the natural lightning (10^{11} W/m). The acoustic radiation from the simulated lightning discharge is characterized by an N-wave with a peak pressure of 2 Pa recorded by microphones at 1.8 m in a 5 kA experiment [22]. This acoustic pressure is on the order of ~ 200 times weaker than that in natural lightning.

3. Analyses of indirect electrode and direct electrode

To eliminate the electrode jet in the laboratory, two types of solutions are developing. The first method is to create an obstruction to the plasma jet and divert the target arc aside with an indirect electrode as shown in Fig. 2a [23,24]. Another solution is to decrease the volume of vaporization of the electrode material with the use of the direct electrode (Fig. 2b) [7,9,25].

The indirect electrode usually uses a ceramic cap with a restricting slit aperture mounted on the head of the electrode that prevents the plasma jet from impinging directly on the testing material (Fig. 2a). It can efficiently divert the target arc aside, but the dielectric cap would absorb partial arc energy and over-pressure wave impacts, meanwhile, it significantly decreases the electric field strength in the vicinity of the electrode tip and reduces the ablation volume on the testing sample. Kern et al. have shown that using the indirect electrode with an insulating Teflon head leads to only 40%~60% of the damage to the sample in comparison with using the direct electrode [25].

In addition, the indirect electrode configuration greatly reduces the air breakdown capability of the cathode/anode, and a metallic ignition wire with a diameter of 0.1~0.2 mm between electrodes is necessarily adopted to create a conductive path and initiate the arc. The ignition wire absorbs energy for melting /evaporation itself, and decreases the energy budget of arc. Concurrently, the consumed wire also generates a considerable volume of metal vapor and contaminates the arc channel. This will increase the diffusion of ions, the net radiative emission
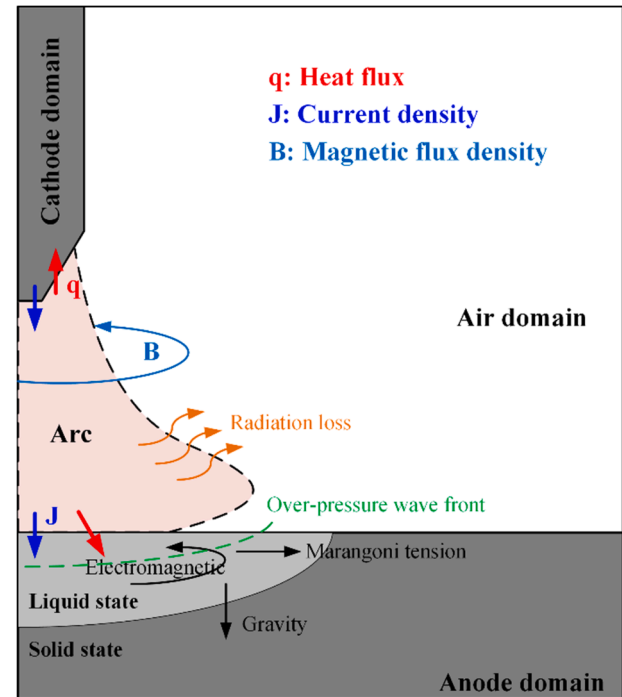

Fig. 3. Cathode-arc-anode domains and the physical interactions.

coefficient, and the electrical conductivity of the plasma column. Therefore, the pinch effects, the heat flux and current density, and the arc radius will be all affected by the undesirable metal vapor [26]. This metal vapor contamination can be clearly inferred from the brighter arc channel observed in the laboratory, as the addition of metal vapor introduces a number of prominent spectral emission lines linked with metal atoms (Cu, W, Al, etc.) [21].

More metal vapor results in a dramatic enhancement in the radiant power density and electrical conductivity, leading to a decrease in the central temperature of the arc [26–28]. This in turn will mitigate the damage effects from the lightning arc. Added metal vapor also plays a role in decreasing the viscosity of the gas and accelerating the axial flow velocity thereafter [29], which flatten the surface heat flux and decrease the damaged depth in the direct lightning testing. The changes in the heat flux and current density and the associated variations in the damaged area and depth of metal (taking Al alloy 3003 as an example) resulting from the lightning continuing current (400A/500ms) are analyzed with the Unified Plasma-Material Finite Element Model (UPM-FEM), which models the arc-material interactions in a domain of the cathode-plasma-anode in the free air with the resistive Magneto-Hydro Dynamics (MHD) method.

As shown in Fig. 3, the lightning arc with a high current is assumed in a local thermodynamic equilibrium (LTE) condition and is regarded as a continuous domain of a thermally and electrically conductive fluid. The
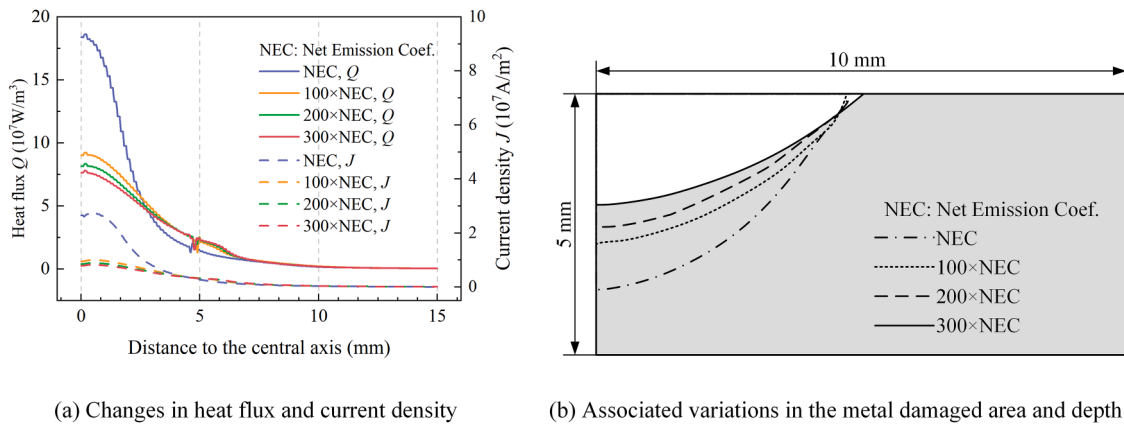
(a) Changes in heat flux and current density

(b) Associated variations in the metal damaged area and depth

Fig. 4. Changes in the heat flux and current density with net emission coefficient and the associated variations in the damaged area and depth of metal resulting from the lightning continuing current.

Table 2
Anti-erosion indices of electrode materials.

Material	T	ρ	c	λ	R
Aluminum	658	2.7	0.90	2.03	1567
Copper	1083	8.9	0.38	4.00	4011
Iron	1527	7.8	0.45	0.82	2581
Tungsten	3415	19.3	0.14	1.70	7257

a) Before arc experiment   b) After arc experiment

Fig. 5. W-Cu direct electrode in blunt conical shape before and after simulated arc experiment.

cathode or anode boundary layers, namely the sheath layers, are stated in the non-LTE discontinuities. In the lightning arc domain, the UPM-FEM sets the governing equations, consisting of the Maxwell's equations, electric current conservation equation, heat transfer energy balance equation, and fluid flow Navier-Stokes equations, and solves these equations in a coupled multiphysics manner. In the cathode or anode domains, Maxwell's equations, electric current conservation equation, and the heat transfer energy balance equation are concurrently considered and then solved. In addition, there are still appreciable electrons and ions participating in ambipolar diffusion of the arc and thermionic emission from the cathode within the boundary layer. The heat flux applied at the anode boundary considers mainly the heating from electron condensation and the radiation cooling loss. The heat flux at the cathode includes the ion heating from collected ions at the cathode, the thermionic cooling for electrons emitted from the cathode, and the radiation cooling loss. A detailed description of the UPM-FEM and its validation is addressed in Liu et al. [30].

As shown in Fig. 4, the increased net emission coefficient (due to the added metal vapor) will significantly decrease the heat flux from 19×10^7 to 6×10^7 W·m^2 and current density from 2.7×10^7 to 0.6×10^7 A·m^2 at the arc attachment point, whereas it brings a moderate enhancement for a radial distance of 3~8 mm far from the arc attachment point on the metal surface. The alterations lead to a decrease in the damaged depth and a slight increase in the damaged area (Fig. 4(c)).

For the direct electrode, an increase in the anti-erosion capability of the electrode material is the key to reducing the electrode melting and decreasing the influence of the electrode jet. The anti-erosion capability is determined by the physical properties of the electrode material, $e.g.$ the melting point, density, specific heat capacity, thermal conductivity, and so on, and can be estimated from Eq. (2) [31]. For the materials commonly used as the discharge electrode, their anti-erosion indices R are shown in Table 2.

$$R = T(\rho c\lambda)^{1/2} \qquad (2)$$

where T is the melting point (°C), ρ is the density (g·cm^{-3}), c is the specific heat capacity (J·g^{-1}·°C^{-1}). λ is the thermal conductivity (W·cm^{-1}·°C^{-1}). R is the anti-erosion index.

Tungsten (W) has the highest anti-erosion index compared with copper, iron, and aluminum (see Table 2). However, the electrical and thermal conductivity of tungsten is very low (its electrical conductivity at 20°C is 1.8×10^7 S/m, about 29% of that of copper), leading to a considerable temperature increase in carrying a large current. Besides tungsten is stiff and so readily susceptible to internal cracking. Improvements are needed to adapt it as an electrode.

Taking the advantage of the superior electrical and thermal conductivity of copper (Cu), the W-Cu alloy can exhibit good characteristics in the melting point, the electrical and thermal conductivity, and the anti-erosion ability, making the alloy most suitable as the electrode material. But the two key materials (W and Cu) are not inter-soluble. To uniformly distribute copper particles inside the tungsten structure, the W-Cu alloy can be manufactured by a special technique, named the copper-infiltrated tungsten skeleton method in a high-temperature atmosphere. This could enhance the conductivity and anti-erosion ability. For the shape design of the electrode, the electrode in a semi-ellipsoidal shape can smooth the surface electric field and alleviate the electrode erosion (Fig. 5), as detailed in [12]. Nevertheless, the core temperature in the simulated arc is higher than 10,000 K and will still cause the electrode to melt or vaporize slightly. Adjustment of the physical properties of the electrode material over the typical range of arc temperature is still a challenge at present.

4. Conclusion

Advantages and drawbacks of the use of a direct electrode or an indirect electrode in simulated lightning damage testing are studied by a combination of simulated lightning experiments and numerical modeling. Results show that,

1) Using the indirect electrode configuration leads to milder damaged area and depth of lightning to materials. Reasons are traced to the dielectric cap on electrode head and the constrained impacts of arc energy and over-pressure wave. Added metal vapor from the ignition wire also alter the net emission coefficient, electrical and thermal conductivity of arc and account for the milder damaged results.

2) The direct electrode configuration can overcome the aforementioned deficiencies but faces an obstacle of self-melting. A special tungsten-copper electrode may be taken as a compromise solution. Adjusting the physical properties of the electrode materials to withstand the high temperature of the arc remains a challenge at present.

3) The peak electric field strength in simulated lightning testing is a factor of 10^3 lower than the counterpart in the natural lightning. The simulated lightning arc generated by means of self-breakdown in the laboratory has consistent optical emission with natural lightning arc. Adoption of multiple currents with representative time sequences and interstroke intervals is recommended for lightning damage testing of materials.

CRediT authorship contribution statement

Y. Liu design of the article. Y. Liu and Y. Wang do the modeling analysis. Y. Liu, C. Xiao, S. Shen conduct the experiment. Y. Liu drafted the article. C. Xiao, S. Shen, Y. Wang, and E. Williams revised it critically.

Declaration of Competing Interest

The authors declare that they have no known competing financial interests or personal relationships that could have appeared to influence the work reported in this paper.

Data availability

Data will be made available on request.

Acknowledgments

References

[1] C. Gomes (Ed.), Lightning: Science, Engineering, and Economic Implications for Developing Countries, Springer, Singapore, Singapore, 2021, https://doi.org/10.1007/978-981-16-3440-6.

[2] V.A. Rakov, M.A. Uman, Lightning: Physics and Effects, Cambridge University Press, Cambridge, U.K. ; New York, 2003.

[3] Y. Liu, Z. Fu, A. Jiang, Q. Liu, B. Liu, FDTD analysis of the effects of indirect lightning on large floating roof oil tanks, Electr. Power Syst. Res. 139 (2016) 81–86.

[4] M.A. Uman, V.A. Rakov, The interaction of lightning with airborne vehicles, Progress in Aerospace Sci. 39 (2003) 61–81, https://doi.org/10.1016/S0376-0421(02)00051-9.

[5] C.C.R. Jones, D. Rowse, G.A.M. Odam, Probabilities of catastrophe in lightning hazard assessments, SAE Technical Paper, 2001.

[6] P. Feraboli, M. Miller, Damage resistance and tolerance of carbon/epoxy composite coupons subjected to simulated lightning strike, Compos. Part A: Appl. Sci. Manuf. 40 (2009) 954–967.

[7] L.I.U. Yakun, F.U. Zhengcai, L.I.U. Quanzhen, L.I.U. Baoquan, G. Anirban, Experimental and analytical investigation on metal damage suffered from simulated lightning currents, Plasma Sci. Technol. 19 (2017), 125301.

[8] M.A. Uman, Natural and artificially-initiated lightning and lightning test standards, Proceed. IEEE 76 (1988) 1548–1565, https://doi.org/10.1109/5.16349.

[9] Y. Liu, A. Guha, J. Montanya, Y. Wang, Z. Fu, Effects of single impulse current and multiwaveform multipulse currents on aluminum alloy in lightning damage analysis, IEEE Trans. Plasma Sci. 48 (2020) 1146–1153, https://doi.org/10.1109/TPS.2020.2977930.

[10] L. Chemartin, P. Lalande, B. Peyrou, A. Chazottes, P.Q. Elias, C. Delalondre, B.G. Cheron, F. Lago, Direct effects of lightning on aircraft structure: analysis of the thermal, Electr. Mech. Constraints (2012), 17.

[11] Y. Wang, Multiphysics analysis of lightning strike damage in laminated carbon/glass fiber reinforced polymer matrix composite materials: A review of problem formulation and computational modeling, Compos. Part A: Appl. Sci. Manuf. 101 (2017) 543–553, https://doi.org/10.1016/j.compositesa.2017.07.010.

[12] Y. Liu, H. Xia, Z. Fu, X. Gao, B. Liu, Analysis on the choosing of test electrode for lightning current metal ablation experiments, in: 2016 33rd International Conference on Lightning Protection (ICLP), Estoril, Portugal, IEEE, 2016, pp. 1–6, https://doi.org/10.1109/ICLP.2016.7791402.

[13] Y.K. Liu, Z.C. Fu, A.F. Jiang, Q.Z. Liu, B.Q. Liu, Analysis and experiment on the influence factor of metal ablation caused by multiple lightning impulse currents, in: Asia-Pacific International Conference on Lightning, Nagoya, Japan, 2015, pp. 736–741 [Sn].

[14] C.P.R. Saunders, A review of thunderstorm electrification processes, J. Appl. Meteorol. 32 (1993) 642–655.

[15] E.R. Williams, The tripole structure of thunderstorms, J. Geophys. Res. 94 (1989), 13151, https://doi.org/10.1029/JD094iD11p13151.

[16] M.A. Uman, Comparison of lightning and a long laboratory spark, Proceed. IEEE 59 (1971) 457–466, https://doi.org/10.1109/PROC.1971.8204.

[17] P. Depasse, Lightning acoustic signature, J. Geophys. Res. 99 (1994), 25933, https://doi.org/10.1029/94JD01986.

[18] API RP 545 - Recommended Practice for Lightning Protection of Aboveground Storage Tanks for Flammable or Combustible Liquids | Engineering360, (n.d.). https://standards.globalspec.com/std/1194265/API%20RP%20545 (accessed March 21, 2022).

[19] ARP5412B: Aircraft Lightning Environment and Related Test Waveforms - SAE International, (n.d.). https://www.sae.org/standards/content/arp5412b/(accessed March 21, 2022).

[20] C.E.R. Bruce, R.H. Golde, The lightning discharge, J. Institution of Electr. Eng.-Part II: Power Eng. 88 (1941) 487–505.

[21] D. Mitchard, D. Clark, D. Carr, A. Haddad, Technique for the comparison of light spectra from natural and laboratory generated lightning current arcs, Appl. Phys. Lett. 109 (2016), 093502, https://doi.org/10.1063/1.4962205.

[22] J. Wang, J. Cao, L. Cai, Y. Fan, M. Zhou, Q. Li, Characteristics of acoustic response from simulated impulsive lightning current discharge, High Voltage 4 (2019) 221–227, https://doi.org/10.1049/hve.2019.0030.

[23] W. Zischank, F. Drumm, R.J. Fisher, G.H. Schnetzer, M.E. Morris, Reliable Simulation of Metal Surface Penetration by Lightning Continuing Currents, Sandia National Labs., Albuquerque, NM (United States), 1995.

[24] H. Maecker, Plasmaströmungen in Lichtbögen infolge eigenmagnetischer Kompression, Zeitschrift Für Physik 141 (1955) 198–216.

[25] A. Kern, Simulation and measurement of melting effects on metal sheets caused by direct lightning strikes, in: Proceedings of International Aerospace and Ground Conference on Lightning and Static Electricity, 1991.

[26] Y. Liu, Y. Wang, Is indirect electrode a good choice for simulated lightning damage tests?—The effect of metal vapor, IEEE Trans. Plasma Sci. 49 (5) (2021) 1661–1668, https://doi.org/10.1109/TPS.2021.3073534.

[27] M. Schnick, U. Füssel, M. Hertel, A. Spille-Kohoff, A.B. Murphy, Metal vapour causes a central minimum in arc temperature in gas–metal arc welding through increased radiative emission, J. Phys. D: Appl. Phys. 43 (2010), 022001, https://doi.org/10.1088/0022-3727/43/2/022001.

[28] M. Tanaka, K. Yamamoto, S. Tashiro, K. Nakata, E. Yamamoto, K. Yamazaki, K. Suzuki, A.B. Murphy, J.J. Lowke, Time-dependent calculations of molten pool formation and thermal plasma with metal vapour in gas tungsten arc welding, J. Phys. D: Appl. Phys. 43 (2010), 434009, https://doi.org/10.1088/0022-3727/43/43/434009.

[29] A.B. Murphy, M. Tanaka, K. Yamamoto, S. Tashiro, T. Sato, J.J. Lowke, Modelling of thermal plasmas for arc welding: the role of the shielding gas properties and of metal vapour, J. Phys. D: Appl. Phys. 42 (2009), 194006, https://doi.org/10.1088/0022-3727/42/19/194006.

[30] Y. Liu, Y. Wang, Modeling the lightning continuing current electric arc discharge and material thermal damage: effects of combinations of amplitude and duration, Int. J. Therm. Sci. 162 (2021), 106786, https://doi.org/10.1016/j.ijthermalsci.2020.106786.

[31] X. Changming, S. Shaohuan, T. Xiaohua, D. Tao, Electrode erosion in high pressure and high current discharges, High Power Laser and Particle Beams 25 (2013) 2181–2187.